2008

Surface Plasmon Resonance Enhanced Transmission of Light through Gold-Coated Diffraction Gratings

Bipin K. Singh
Iowa State University

Andrew C. Hillier
Iowa State University, hillier@iastate.edu

Anal. Chem. **2008,** *80,* 3803–3810

Surface Plasmon Resonance Enhanced Transmission of Light through Gold-Coated Diffraction Gratings

Bipin K. Singh and Andrew C. Hillier*

Department of Chemical and Biological Engineering and Department of Chemistry, Iowa State University, Ames, Iowa 50011

Narrow peaks are observed in the transmission spectra of p-polarized light passing through a thin gold film that is coated on the surface of a transparent diffraction grating. The spectral position and intensity of these peaks can be tuned over a wide range of wavelengths by simple rotation of the grating. The wavelengths where these transmission peaks are observed correspond to conditions where surface plasmon resonance occurs at the gold−air interface. Light diffracted by the grating couples with surface plasmons in the metal film to satisfy the resonant condition, resulting in enhanced light transmission through the film. Notably, this phenomenon is not observed at flat, gold-coated surfaces or uncoated gratings, where coupling to surface plasmons does not occur. The nature of the coupling and, thus, the details of light transmission are governed by the momentum matching conditions between the diffracted light and the surface plasmons. In the presence of bound analytes or surface films, the enhanced transmission peaks are red-shifted, making a simple, yet highly responsive sensing platform. The utility of this platform is demonstrated for ex situ sensing by analyzing thin films of various thicknesses and detecting a model immunoreaction between bovine serum albumin and anti-bovine serum albumin. This grating-based transmission surface plasmonic device represents a simple and sensitive platform, which can be readily tuned to enhance performance and be used in the study of a variety of surface adsorption processes or analysis of biomolecular interactions.

Sensors based on surface plasmon resonance (SPR) have become increasingly popular as a label-free method for measuring the binding of analytes to functionalized surfaces and in the detection of immobilized biomolecules. SPR sensing has been exploited in the development of immunosensors,[1–3] advancing proteomics,[4,5] accelerating drug discovery,[6,7] monitoring DNA hybridization,[8,9] and detecting protein−DNA interactions.[10,11] Several reviews of SPR-based sensing techniques have been published.[11–15] The large field-enhancement associated with SPR is also the basis for many surface analytical techniques such as surface-enhanced Raman scattering,[16] surface-enhanced fluorescence,[17] surface plasmon-enhanced diffraction,[18–20] and surface-enhanced infrared absorption spectroscopy.[21,22] One of the key attributes of SPR sensing is that it eliminates the complex labeling/conjugation steps required of competing techniques that utilize fluorescently labeled molecules in detection assays.[23]

In a typical SPR-based immunoassay, one of the molecules of an interacting pair is immobilized near a metal surface using appropriate surface chemistry. When the complementary molecule binds with the immobilized species, it increases the refractive index near the metal surface. This induces a change in the surface plasmon resonance condition and, hence, impacts the characteristics of the interacting light. Monitoring light in reflection[14] or

* To whom correspondence should be addressed. E-mail: hillier@iastate.edu.

(1) Nishimura, T.; Hifumi, E.; Fujii, T.; Niimi, Y.; Egashira, N.; Shimizu, K.; Uda, T. *Electrochemistry* **2000**, *68*, 916–919.
(2) Mullett, W. M.; Lai, E. P. C.; Yeung, J. M. *Methods* **2000**, *22*, 77–91.
(3) Hsieh, H. V.; Stewart, B.; Hauer, P.; Haaland, P.; Campbell, R. *Vaccine* **1998**, *16*, 997–1003.
(4) Oda, Y.; Owa, T.; Sato, T.; Boucher, B.; Daniels, S.; Yamanaka, H.; Shinohara, Y.; Yokoi, A.; Kuromitsu, J.; Nagasu, T. *Anal. Chem.* **2003**, *75*, 2159–2165.
(5) Wilkinson, F. L.; Holaska, J. M.; Zhang, Z. Y.; Sharma, A.; Manilal, S.; Holt, I.; Stamm, S.; Wilson, K. L.; Morris, G. E. *Eur. J. Biochem.* **2003**, *270*, 2459–2466.
(6) Rich, R. L.; Day, Y. S. N.; Morton, T. A.; Myszka, D. G. *Anal. Biochem.* **2001**, *296*, 197–207.
(7) Baird, C. L.; Courtenay, E. S.; Myszka, D. G. *Anal. Biochem.* **2002**, *310*, 93–99.
(8) Nilsson, P.; Persson, B.; Uhlen, M.; Nygren, P. A. *Anal. Biochem.* **1995**, *224*, 400–408.
(9) Peterlinz, K. A.; Georgiadis, R. M.; Herne, T. M.; Tarlov, M. J. *J. Am. Chem. Soc.* **1997**, *119*, 3401–3402.
(10) Gotoh, M.; Hasebe, M.; Ohira, T.; Hasegawa, Y.; Shinohara, Y.; Sota, H.; Nakao, J.; Tosu, M. *Genet. Anal.-Biomol. Eng.* **1997**, *14*, 47–50.
(11) Silin, V.; Plant, A. *Trends Biotechnol.* **1997**, *15*, 353–359.
(12) Green, R. J.; Frazier, R. A.; Shakesheff, K. M.; Davies, M. C.; Roberts, C. J.; Tendler, S. J. B. *Biomaterials* **2000**, *21*, 1823–1835.
(13) Lechuga, L. M.; Calle, A.; Prieto, F. *Quim. Anal.* **2000**, *19*, 54–60.
(14) Homola, J.; Koudela, I.; Yee, S. S. *Sens. Actuators, B* **1999**, *54*, 16–24.
(15) Homola, J. *Anal. Bioanal. Chem.* **2003**, *377*, 528–539.
(16) Nie, S. M.; Emery, S. R. *Science* **1997**, *275*, 1102–1106.
(17) Lakowicz, J. R.; Geddes, C. D.; Gryczynski, I.; Malicka, J.; Gryczynski, Z.; Aslan, K.; Lukomska, J.; Matveeva, E.; Zhang, J. A.; Badugu, R.; Huang, J. *J. Fluoresc.* **2004**, *14*, 425–441.
(18) Yu, F.; Tian, S. J.; Yao, D. F.; Knoll, W. *Anal. Chem.* **2004**, *76*, 3530–3535.
(19) Tian, S. J.; Armstrong, N. R.; Knoll, W. *Langmuir* **2005**, *21*, 4656–4660.
(20) Wark, A. W.; Lee, H. J.; Qavi, A. J.; Corn, R. M. *Anal. Chem.* **2007**, *79*, 6697–6701.
(21) Leverette, C. L.; Jacobs, S. A.; Shanmukh, S.; Chaney, S. B.; Dluhy, R. A.; Zhao, Y. P. *Appl. Spectrosc.* **2006**, *60*, 906–913.
(22) Williams, S. M.; Stafford, A. D.; Rodriguez, K. R.; Rogers, T. M.; Coe, J. V. *J. Phys. Chem. B* **2003**, *107*, 11871–11879.
(23) Rucker, V. C.; Havenstrite, K. L.; Herr, A. E. *Anal. Biochem.* **2005**, *339*, 262–270.

10.1021/ac800045a CCC: $40.75
Published on Web 04/10/2008

transmission[24] modes is a common method to observe SPR. At appropriate conditions, a reduction in the intensity for wavelengths that satisfy the SPR condition is observed. However, it has recently been discovered that the transmission of specific wavelengths of light at nanostructured surfaces, such as nanometer-sized hole and slit arrays, can be enhanced by SPR.[25] This phenomenon is termed "extraordinary optical transmission" because the observed transmitted light intensity is much higher than what would be expected based on classical aperture theory. For the case of nanohole arrays, the nanoholes serve to convert photons into plasmons on one side of the metal film, which then tunnel through to the other side where they are converted back into photons. An explanation for this phenomena based upon optical tunneling has been proposed,[26] and it forms the basis for a variety of emerging photonic devices.[27]

Since surface plasmons play an important role in the transmission of light through nanohole arrays, the magnitude and position of these enhanced transmission peaks are sensitive to refractive index changes near the surface, which allows it to detect molecular binding events in a sensor format. For example, sensors have been developed based on the transmission peaks observed at a single nanohole[28] or nanohole[29–32] and nanoslit[33] arrays. These sensors have distinct advantages over conventional SPR sensing schemes. For example, sensors in which a decrease in the reflected light intensity is measured can be strongly affected by noise. In contrast, monitoring enhanced transmission improves signal-to-noise by presenting a bright spot on a dark background. Also, these transmission measurements can be performed in a simple collinear geometry where the light source, sample, and detector can be aligned to form a straight line, which avoids the requirement of precise angular alignment as in conventional SPR sensors. However, one major limitation of nanostructured sensors is the need for complex and high resolution machining processes to create the subwavelength topographical features.

Gratings represent simple nanostructured surfaces that have previously been exploited for surface plasmon biosensing either as ex situ or in situ platforms. These sensor schemes have relied either on specular reflection[34] or direct measurement of the diffracted peaks generated at patterned[18,19] or prism-coupled surfaces.[20] In this work, a simple platform based upon an inexpensive and commercially available diffraction grating is exploited to perform transmission-based sensing that relies upon surface plasmon-generated extraordinary optical transmission. A transparent diffraction grating is modified with a thin gold film and illuminated with p-polarized white light. Enhanced light transmission is observed over a narrow wavelength range corresponding to conditions that excite surface plasmons at the gold−air interface. Indeed, it has been recently shown that nanoscale perforations are not necessary for enhanced transmission and peaks in transmitted light can be observed through continuous metal films.[17,30,35,36] We explore the nature of these transmission peaks in this work to identify the origins of the enhanced transmission as well as the impact of illumination angle on the observed peaks. In addition, the utility of this device as an ex situ sensor is demonstrated by measuring the thickness of various thin films. A model immunosensing application is also examined involving the formation of immunocomplexes between bovine serum albumin (BSA) and anti-BSA. This work demonstrates the utility and versatility of this grating-based SPR sensing technique.

EXPERIMENTAL SECTION

Materials and Reagents. Absolute ethanol, 11-mercaptoundecanoic acid (MUA), hexanethiol (HT), decanethiol (DT), octadecanethiol (ODT), BSA, polyclonal rabbit anti-BSA, *N*-hydroxysuccinimide (NHS), *N*-(3-dimethylaminopropyl)-*N*′-ethylcarbodiimide hydrochloride (EDC), and 4-(2-hydroxyethyl)-1-piperazineethanesulfonic acid (HEPES) were purchased from Sigma Aldrich (St. Louis, MO). All chemicals and reagents were used as received. Recordable digital versatile discs (DVD-R, 4.7GB) were purchased from Inkjet Art Solutions (Salt Lake City, UT). Gold (99.999%) was purchased from Ernest Fullam (Latham, NY). HEPES-buffered saline (HBS) was prepared with the pH adjusted to 7.4 using 10 mM NaOH and stored at 4 °C. All buffers and solutions were prepared with 18 MΩ cm deionized water (NANOPure, Barnstead, Dubuque, IA).

Grating Construction. The DVD-Rs used in this work are single-sided and single-layered with a storage capacity of 4.7 GB. The DVD-Rs consist of two 0.6 mm thick circular polycarbonate pieces that sandwich a reflective metal and a dye layer between them (see Supporting Information). One of the polycarbonate pieces possesses a continuous spiral groove formed during the injection molding process that assists in laser tracking during writing and recovery of data. This polycarbonate piece forms the clear face of the DVD-R. A photosensitive dye is coated on top of the groove, which is what is "burned" in the process of writing data on a DVD-R. A thin (50−100 nm) layer of reflective metal is sputtered on top of the dye layer followed by another protective 0.6 mm polycarbonate cover piece to prevent physical damage to the metal and dye layers. We utilized the grooved polycarbonate layer in a DVD-R as an inexpensive source of high quality plastic diffraction gratings. We have previously described the construction of grating-based SPR sensing chips derived from recordable compact discs (CD-Rs).[34]

For preparation of the gratings, the DVD-R was manually split into two constituent polycarbonate pieces at the center-plane using a razor blade. The grooved polycarbonate piece is easily distinguishable from the unstructured polycarbonate piece as it exhibits a "rainbow" of diffracted light and has a blue tint due to the dye layer. The dye is readily removed from the piece by washing in ethanol followed by drying in a stream of nitrogen. The dried

(24) Lochbihler, H. *Phys. Rev. B* **1994**, *50*, 4795–4801.
(25) Ebbesen, T. W.; Lezec, H. J.; Ghaemi, H. F.; Thio, T.; Wolff, P. A. *Nature* **1998**, *391*, 667–669.
(26) Darmanyan, S. A.; Zayats, A. V. *Phys. Rev. B* **2003**, *67*, 035424.
(27) Muhlschlegel, P.; Eisler, H. J.; Martin, O. J. F.; Hecht, B.; Pohl, D. W. *Science* **2005**, *308*, 1607–1609.
(28) Rindzevicius, T.; Alaverdyan, Y.; Dahlin, A.; Hook, F.; Sutherland, D. S.; Kall, M. *Nano Lett.* **2005**, *5*, 2335–2339.
(29) Brolo, A. G.; Arctander, E.; Gordon, R.; Leathem, B.; Kavanagh, K. L *Nano Lett.* **2004**, *4*, 2015–2018.
(30) Kats, A. V.; Nikitin, A. Y. *Phys. Rev. B* **2004**, *70*, 235412.
(31) Stark, P. R. H.; Halleck, A. E.; Larson, D. N. *Methods* **2005**, *37*, 37–47.
(32) Tetz, K. A.; Pang, L.; Fainman, Y. *Opt. Lett.* **2006**, *31*, 1528–1530.
(33) Jung, Y. S.; Sun, Z.; Wuenschell, J.; Kim, H. K.; Kaur, P.; Wang, L.; Waldeck, D. *Appl. Phys. Lett.* **2006**, *88*, 243105.
(34) Singh, B. K.; Hillier, A. C *Anal. Chem.* **2006**, *78*, 2009–2018.
(35) Bai, B. F.; Li, L. F.; Zeng, L. J. *Opt. Lett.* **2005**, *30*, 2360–2362.
(36) Gerard, D.; Salomon, L.; de Fornel, F.; Zayats, A. V. *Phys. Rev. B* **2004**, *69*, 113405.

grating is then placed in a vacuum chamber for deposition of a gold film (Denton Vacuum Turbo III, Morrestown, NJ). Gold is deposited onto the gratings at a rate of 1−2 Å s^{-1} and a pressure of 7×10^{-5} Torr under nitrogen atmosphere to a desired thickness between 20 and 50 nm.

Atomic Force Microscope (AFM) Imaging. AFM images of the sample surfaces were acquired with a Dimension 3100 scanning probe microscope and Nanoscope IV controller (Veeco Metrology, LLC, Santa Barbara, CA). Imaging was performed in the tapping mode using silicon TESP7 AFM tips (Veeco Metrology, LLC, Santa Barbara, CA) with a spring constant of ~70 N m^{-1} and a resonance frequency of ~280 kHz.

Formation of Thin Films. Gold gratings were immersed in 2 mM ethanolic solutions of MUA, HT, DT, or ODT for 24 h. The gratings were subsequently rinsed with ethanol to remove unbound thiol and dried in nitrogen. Activation of carboxylic acid terminated surfaces of MUA was achieved by exposing the sample to an aqueous solution containing 150 mM EDC and 30 mM NHS for 45 min. This reaction resulted in the formation of reactive succinimide esters on the surface, which can combine with primary amine groups of a protein molecule and form a peptide bond with the MUA layer on the surface. Attachment of BSA to the modified MUA surface was achieved by exposing the surface to 0.5 mg mL^{-1} solution of BSA in HBS for 2 h. The sample was then rinsed briefly with HBS to remove unbound BSA and dried.

Formation of Antigen−Antibody Complexes. Gratings with covalently attached BSA films were successively immersed for 3 h in solutions containing 1, 5, 20, 50, 100, 200, and 500 μg mL^{-1} (or equivalently 7 nM, 33 nM, 0.13 μM, 0.33 μM, 0.67 μM, 1.33 μM, and 3.3 μM) of anti-BSA in HBS. The sample was gently removed and dried between each incubation step. Complexation on the sample was measured using both ellipsometry and optical transmission in air. The nonspecific adsorption of BSA antibodies was tested on MUA covered gold gratings by immersing it in the 500 μg mL^{-1} solution of anti-BSA for 3 h. No notable absorption occurred.

Ellipsometry. Film thicknesses for the various samples were measured using ellipsometry. In order to avoid having the diffracted peaks interfere with the ellipsometry measurements, the grating was rotated by 90° so that the grooves in the substrate were orthogonal to the ellipsometer's light path. A motorized variable-angle null ellipsometer (Multiskop, Optrel GbR) operating in the polarizer-compensator-sample-analyzer (PCSA) configuration utilizing a single wavelength (632.8 nm) at 70° angle of incidence was used to measure the ellipsometric parameters Δ and Ψ. The values of Δ and Ψ were converted into equivalent optical thicknesses using a three-medium model. The optical constants of the gold substrate (refractive index n and the absorption coefficient k) were first determined using a two-phase model (air−substrate). The thickness of the adsorbed film was then found using a three-phase model (air−film−substrate) with a value of 1.45 selected for the refractive index of the SAMs[37] as well as protein films.[38]

UV−Visible Transmission Spectroscopy. All optical transmission measurements were carried out in a collinear geometry. White light from a halogen source (model LS1, Ocean Optics, Dunedin, FL) was collimated using a convex lens with focal length of 150 mm (Newport Corp.). The resulting beam passed through a linear polarizer before illuminating the grating sample through a 2 mm diameter aperture. The sample was mounted on a rotating sample holder for manual alignment. The transmitted light was collected by a 600 μm optical fiber and recorded with a fiber optic spectrometer (SD2000, Ocean Optics, Inc., Dunedin, FL). Each spectrum consisted of the average of 100 individual spectra, which were further processed in MATLAB using the RLOESS smoothing function.[39]

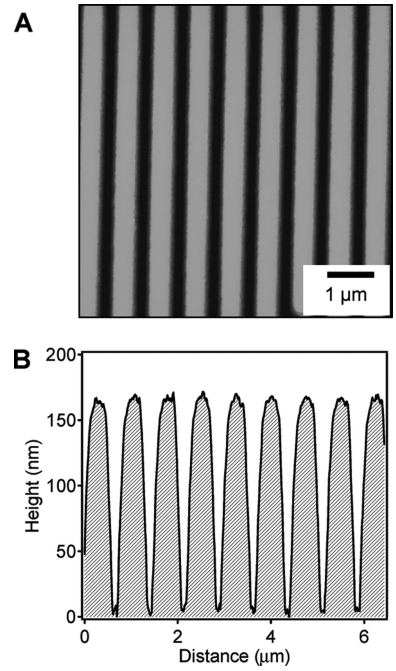

Figure 1. (A) AFM image (6.4 μm × 6.4 μm) of the topography of gold-coated grating constructed from commercial DVD-R. (B) Cross-sectional profile of grating surface.

RESULTS AND DISCUSSION

The gold-coated substrates used in this study were constructed by depositing a transparent gold film of between 20 and 50 nm thickness onto gratings derived from commercial DVD-Rs (see Supporting Information). Figure 1A shows the topography of the gold-coated gratings prepared by this method. The cross-sectional profile indicates a grating pitch of 743 nm and amplitude of 165 nm (Figure 1B). Roughness analysis of the gold coating revealed a smooth surface with a typical root-mean-square (rms) roughness of 2.1 nm over an area of 1 μm^2.

UV−vis transmission spectra were measured through the gold-coated gratings using a custom-built apparatus (Figure 2). A collimated beam of white light illuminated the sample over a 2 mm diameter spot size after passing through a linear polarizer, which allowed the polarization state of light to be varied between p and s. The light transmitted through the grating was collected by a 600 μm diameter optical fiber and analyzed with a UV−vis spectrometer. The grating was mounted on a rotation stage to allow for transmission measurements of the zeroth order beam at different angles of incidence, θ, while keeping the light and collection optics stationary in a collinear geometry.

(37) Bain, C. D.; Troughton, E. B.; Tao, Y. T.; Evall, J.; Whitesides, G. M.; Nuzzo, R. G. *J. Am. Chem. Soc.* **1989**, *111*, 321–335.

(38) Benesch, J.; Askendal, A.; Tengvall, P. *Colloids Surf., B* **2000**, *18*, 71–81.

(39) Cleveland, W. S.; Devlin, S. J. *J. Am. Stat. Assoc.* **1988**, *83*, 596–610.

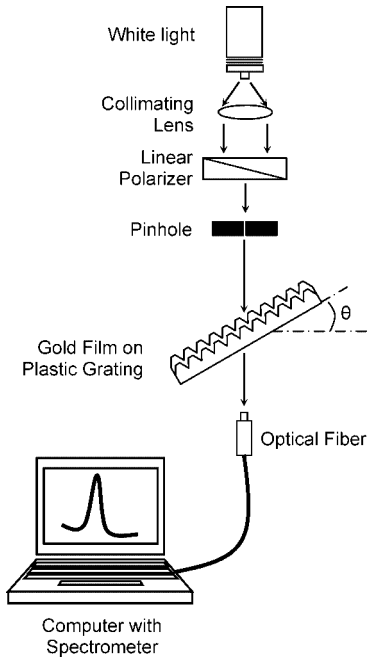

Figure 2. Schematic illustrating the experimental setup used for measuring the transmission spectra through grating samples.

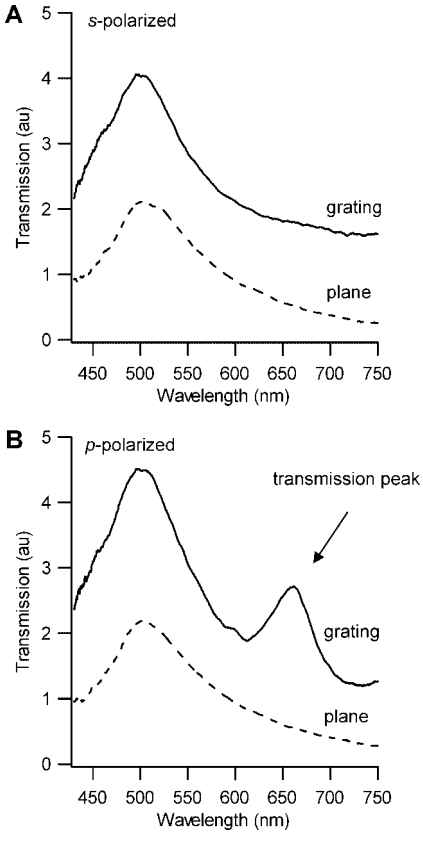

Figure 3. Transmission spectra at $\theta = 50°$ for 45 nm thick gold film with (A) s-polarized and (B) p-polarized light on a flat surface (dashed line) and grating (solid line). The curves have been offset for clarity.

Parts A and B of Figure 3 depict the transmission spectra for s- and p-polarized white light with the sample rotated at an angle of $\theta = 50°$. The data show transmission results for both a grating and a planar surface coated with 45 nm of gold. The response

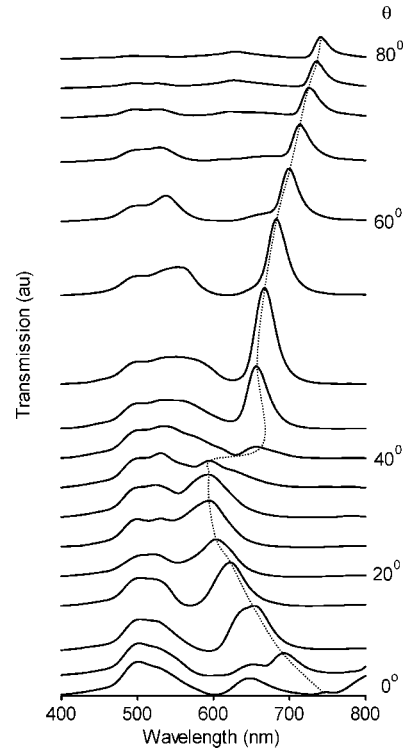

Figure 4. Transmission of p-polarized light through a 45 nm gold film on the grating for angle of incidence $\theta = 0°$, 5°, 10°,..., 80°. The dotted line is plotted as a guide to show the maxima in the enhanced transmission peaks.

measured through the planar gold film for both s- and p-polarized light shows a broad peak near 500 nm, which is consistent with the green transmitted color of transparent gold films. The s-polarized light through the gold-coated grating shows a similar response. However, an additional peak is observed at ~670 nm in the spectra for the p-polarized light transmitted through the grating (Figure 3B). The increased light transmission for this peak represents an enhancement of ~60% over the similar spectrum through a planar sample. The location of this transmission peak, as well as the magnitude of the peak was found to vary with the angle of incidence as well as the details of the gold film and grating.

Manipulating the angle of the grating with respect to the incident light had a large impact on both the magnitude and wavelength of the transmission peak. Figure 4 shows the transmission spectra for p-polarized white light through a gold-coated grating for rotation angles between $\theta = 0°$ and 80°. In addition to the normal transmission spectrum of gold localized in the region between 450 and 550 nm, additional peaks are apparent. Notably, these additional peaks are absent in similar measurements on a planar surface and also with s-polarized light through the grating. At $\theta = 5°$, a peak is apparent at ~700 nm, which shifts to shorter wavelengths as θ is increased. As the angle of incidence is increased from 5° up to 25°, the peak is green-shifted toward a value of ~600 nm. In addition, the magnitude of the peak increases as the angle is increased from 5° to 15° and then decreases in magnitude before vanishing at ~40°. A further increase in θ above 40° results in the appearance of a strong transmission peak at 630 nm. As the angle of incidence is increased, this peak shifts to higher wavelengths. A maximum in the peak intensity is observed

at ~50°, before decreasing in size and then vanishing as the grazing angle is approached.

To understand the nature and origins of these peaks in the transmission spectra, we investigated the possible role of surface plasmons (SPs). Optical excitation of surface plasmons (SPs) at a metal−dielectric interface requires matching of the momentum of the incident light and the SPs. Since momentum and wavevector differ by a constant multiplying factor, an equivalent condition is to say that photons can couple to SPs when the surface-parallel component of the wavevector of incident light ($k_{||}$) matches that of the SPs. The SPs have a complex wavevector k_{sp}, the real part of which (k'_{sp}) is described by the following dispersion relationship:[40]

$$k'_{sp} = \frac{2\pi}{\lambda}\sqrt{\frac{\varepsilon'_M \varepsilon_D}{\varepsilon'_M + \varepsilon_D}} \quad (1)$$

where λ is the wavelength of excitation while $\varepsilon_M = (\varepsilon'_M + \varepsilon'_M)$ and ε_D are the dielectric constants of the metal and dielectric layers. Since the momentum of incident light in air is lower than that given by eq 1, a coupling device is needed.[40] For a periodically modulated interface such as a grating between a metal and a dielectric with a period (or pitch) Λ, the surface component of the wavevector of incident light can be increased (or decreased) by integral multiples of the grating wavevector. If the magnitude of the grating wavevector matches that of SPs in the metal, it can excite them. Mathematically, this relationship is expressed by

$$k'_{sp} = \frac{2\pi}{\lambda}\sqrt{\frac{\varepsilon'_M \varepsilon_D}{\varepsilon'_M + \varepsilon_D}} = \frac{2\pi}{\lambda}\sqrt{\varepsilon_D}\ \sin\theta + m\frac{2\pi}{\Lambda} = k_{||} \quad (2)$$

where θ is angle of incidence and m is an integer (0, ±1, ±2,...) indicating the diffracted order. A reasonable approximation included in eq 2 is that the dispersion relationship of the SPs on a modulated metal surface is same as that on a flat metal surface.[40] A more complete model would take into account the squared dependence of the angular red-shift in the SPR minimum on the amplitude of grating modulation. For the gratings used in this study, this shift is small (>0.1°) and, thus, is ignored during further analysis.[41]

A graphical solution for eq 2 is depicted in Figure 5. In parts A and B of Figure 5, the dashed line represents the dispersion relation of the SPs (eq 1) while the solid lines represent the energy of the in-plane component of the grating wavevector ($k_{||}$) for diffracted orders $m = 0, \pm1, \pm2$ at rotation angles of $\theta = 0°$ (Figure 5A) and $\theta = 90°$ (Figure 5B). As depicted in Figure 5A, the intersection of the dashed and solid lines represent solutions to eq 2 at $\theta = 0°$. As θ is increased, $k_{||}$ increases by an amount that is proportional to ($\sin\theta/\lambda$). Graphically, this is equivalent to tilting the lines for the grating energy. The limiting case of $\theta = 90°$ is depicted in Figure 5B. The graphical solution also indicates that the wavelength where coupling occurs with the SPs decreases for positive diffracted orders ($m > 0$) or increases for negative diffracted orders ($m < 0$) as θ is increased.

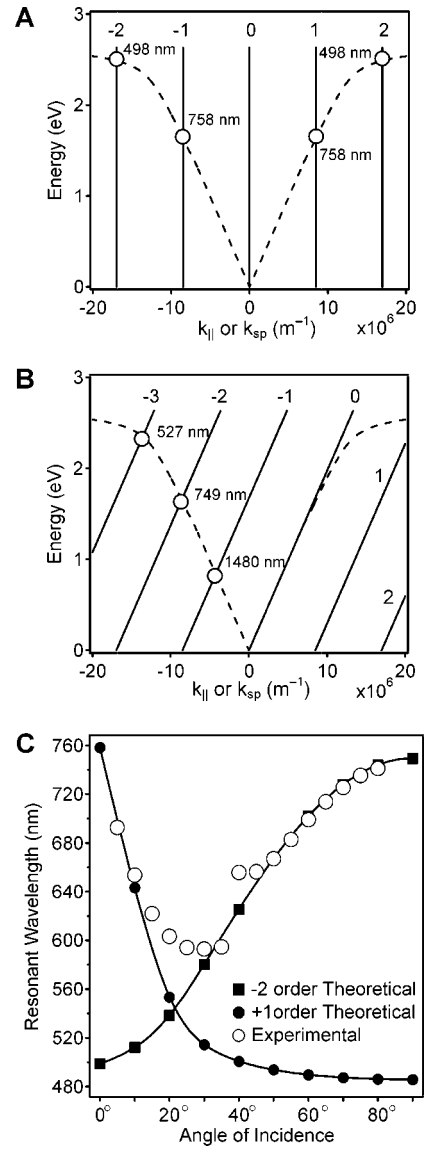

Figure 5. (A) Graphical solution to eq 2, at $\theta = 0°$ and $\Lambda = 740$ nm, corresponding to intersection of the plasmon dispersion curve k_{sp} (dashed line) and the light wave vector $k_{||}$ (solid line) as it varies with the diffracted order ($m = -3, -2, -1, 0, 1, 2$). (B) Graphical solution physically at a grazing angle of $\theta = 90°$. (C) Wavelength corresponding to graphical solution as a function of the angle of incidence for $n = -2$ and $+1$ diffracted order.

A series of solutions to eq 2 were determined with similar plots generated at different angles of incidence. The resulting solutions are illustrated in Figure 5C for the $m = +1$ and $m = -2$ diffracted orders. The position of the experimentally measured transmission peaks from Figure 4 are also plotted on this curve. There is a clear overlap between the measured transmission peaks and those determined from the solutions to eq 2. This suggests that the origin of the enhanced transmission peaks is from excitation of surface plasmons in the gold film at these conditions. Specifically, at angles between 0 and ~40°, excitation is from the $m = +1$ diffracted order, while at larger angles, excitation is due to the $m = -2$ diffracted order.

(40) Raether, H. *Surface Plasmons on Smooth and Rough Surfaces and on Gratings*; Springer-Verlag: New York, 1988.
(41) Raether, H. *Opt. Commun.* **1982**, *42*, 217–222.
(42) Schroter, U.; Heitmann, D. *Phys. Rev. B* **1999**, *60*, 4992–4999.
(43) Bonod, N.; Enoch, S.; Li, L. F.; Popov, E.; Neviere, M. *Opt. Express* **2003**, *11*, 482–490.

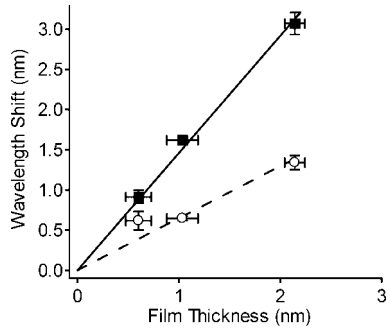

Figure 6. Experimentally measured wavelength shifts in the transmission spectra at $\theta = 15°$ (■) and 50° (○) versus ellipsometrically measured thicknesses for thin films consisting of hexanethiol (HT), decanethiol (DT), and octadecanethiol (ODT).

A similar correlation between peaks in the transmission spectra and excitation of SPs has been previously reported.[42] Theoretical investigations have revealed that enhanced transmission can occur through modulated metal films.[43] Moreover, the SPs are transverse magnetic in nature, which means that they can only be excited by p-polarized light. This polarization dependent transmission behavior is clearly shown by Figure 3, which further reinforces the hypothesis regarding the dominant role of SPR in the enhanced light transmission.

We further investigated the response of these peaks in the presence of thin surface films and adsorbates in order to test the ability of this system to serve as a sensing platform. As a first step, we utilized ω-functionalized *n*-alkanethiols ($HS-(CH_2)_n-X$) to chemically modify the gold grating surface with a well-defined set of monolayer films.[44] Self-assembled monolayers of hexanethiol (HT) ($n = 5$, $X = CH_3$), decanethiol (DT) ($n = 9$, $X = CH_3$) and octadecanethiol (ODT) ($n = 17$, $X = CH_3$) were each coated onto the gold gratings. The position of the transmission peak was measured for the gratings with HT, DT, and ODT films. The transmission was measured at sample rotation angles of $\theta = 15°$ and 50°, which represent the locations of the peak maximum for the $m = +1$ and -2 diffracted orders.

The spectra obtained for transmission of s-polarized light in the presence of these films were unchanged compared to the uncoated grating for all of the samples. However, for p-polarized light the enhanced transmission peaks were shifted to longer wavelengths. Although modeling the results from typical Kretschmann-type SPR sensors is straightforward, solving Maxwell's equations for a surface−film−ambient interface at gratings is much more complex and beyond the scope of this work. Therefore, ellipsometry was used to compare the peak shifts with the thicknesses of the monomolecular films. The measured thicknesses of the HT, DT, and ODT films were 0.60, 1.04, and 2.14 nm, which are comparable to literature reports for densely packed alkanethiolate monolayers formed out of ethanolic solutions.[37,45] As noted in Figure 6 and Table 1, the $m = +1$ (15°) and $m = -2$ (50°) peaks both shifted toward longer wavelengths with increasing film thickness. This shift was linear for both. Using a more complete set of films of thickness ranging from 0 up to ~11 nm (see Table 1, Table 2 and Supporting Information), we determine calibration constants of 1.38 nm shift/nm thickness for the $m = +1$ peak and 0.75 nm shift/nm thickness for the $m = -2$ peak. Thus, the $m = +1$ peak exhibits a higher sensitivity to film thickness than the $m = -2$ peak. A comparison of the sensitivity of this SPR sensing platform can be provided in terms of refractive index units using eq 2 for a direct comparison with other SPR based methods. The sensitivity of this SPR sensing method corresponds to ~600 nm RIU^{-1}, which is comparable to those calculated for grating-based (300−630 nm RIU^{-1})[46] and nanostructure-based (150−400 nm RIU^{-1})[14,47] SPR sensors.

After confirming that the transmission peaks are sensitive to the thickness of films present at the grating surface, we explored the utility of this detection method in an immunosensing platform. BSA and anti-BSA were chosen as a model antigen−antibody system. This model system has routinely been used to demonstrate the performance of SP-based sensing platforms such as differential phase measurement SPR,[35] SPR spectroscopy,[48] and localized SPR.[49] A first step in the construction of the immunosensor was the modification of the gold grating surface with a self-assembled monolayer of mercaptoundecanoic acid (MUA) ($n = 10$, $X =$ COOH). MUA is a convenient choice for covalent immobilization of proteins using an amine coupling method.[50] The COOH surface of MUA can be activated to form reactive NHS esters that readily react with pendant primary amine groups that are commonly found in proteins.[51] Clean gold gratings were incubated in 2 mM MUA ethanolic solutions for 24 h and then washed with ethanol and dried under nitrogen. The samples were then immersed in an aqueous NHS−EDC solution for 45 min. After a brief wash with deionized water, the samples were immersed in a 0.5 mg mL^{-1} solution of BSA in HBS for 2 h. This coupling step attached BSA to the SAM on gold via the formation of covalent amide bonds. Covalently attached BSA molecules have been shown to retain their antigenicity upon their immobilization at a solid surface.[49] The samples with immobilized BSA films were rinsed and incubated for 3 h sequentially in solutions containing 1, 5, 20, 50, 100, 200, and 500 μg mL^{-1} of anti-BSA at room temperature of 21 °C. The samples were dried after each surface modification step, and then transmission and ellipsometry measurements were carried out (Table 2). The thickness of the covalently attached BSA film was measured to be 3.54 nm (minus the MUA layer), which is similar to values reported in literature[34,52] and agrees well with the 14 nm × 4 nm × 4 nm ellipsoidal shape of BSA.[53] The complete thickness of the fully formed film of antigen−antibody complexes was 9.74 nm (minus the MUA layer), which agrees well with the dimensions of antigen−antibody complexes measured by AFM[54] and the thickness of a film made up of antigen−antibody complexes.[55] Notably, a set of control MUA-covered gratings were immersed in the 500 μg mL^{-1}

(44) Sullivan, T. P.; Huck, W. T. S. *Eur. J. Org. Chem.* **2003**, *17*, 29.
(45) Porter, M. D.; Bright, T. B.; Allara, D. L.; Chidsey, C. E. D. *J. Am. Chem. Soc.* **1987**, *109*, 3559–3568.
(46) Moharam, M. G.; Gaylord, T. K. *J. Opt. Soc. Am. A* **1986**, *3*, 1780–1787.
(47) Malinsky, M. D.; Kelly, K. L.; Schatz, G. C.; Van Duyne, R. P. *J. Am. Chem. Soc.* **2001**, *123*, 1471–1482.
(48) Akimoto, T.; Sasaki, S.; Ikebukuro, K.; Karube, I. *Biosens. Bioelectron.* **2000**, *15*, 355–362.
(49) Fujiwara, K.; Watarai, H.; Itoh, H.; Nakahama, E.; Ogawa, N. *Anal. Bioanal. Chem.* **2006**, *386*, 639–644.
(50) Johnsson, B.; Lofas, S.; Lindquist, G. *Anal. Biochem.* **1991**, *198*, 268–277.
(51) Patel, N.; Davies, M. C.; Hartshorne, M.; Heaton, R. J.; Roberts, C. J.; Tendler, S. J. B.; Williams, P. M. *Langmuir* **1997**, *13*, 6485–6490.
(52) Brynda, E.; Houska, M. *J. Colloid Interface Sci.* **1996**, *183*, 18–25.
(53) Peters, T. *Adv. Protein Chem.* **1985**, *37*, 161–245.

Table 1. List of Thicknesses and Shifts in Transmission Peak for HT, DT, and ODT Self-Assembled Monolayers on Gold Gratings

surface	red shift in peak location with respect to bare gold at 15° (nm)	red shift in peak location with respect to bare gold at 50° (nm)	ellipsometric thickness (nm)
Au/HT	0.91	0.62	0.60
Au/DT	1.62	0.65	1.04
Au/ODT	3.07	1.34	2.14

Table 2. Measured Film Thicknesses and Shifts in Transmission Peak during Formation of MUA Self-Assembled Monolayer, Covalent Immobilization of BSA, and Formation of Antigen−Antibodies Complexes on the Grating Surface upon Exposure to Anti-BSA Solutions

surface	red shift in peak location with respect to bare gold at 15° (nm)	red shift in peak location with respect to bare gold at 50° (nm)	ellipsometric thickness (nm)
Au/MUA	2.21	1.03	1.34
Au/MUA/BSA	6.57	3.55	4.88
Au/MUA/BSA + 1 μg/mL anti-BSA	8.11	4.11	5.82
Au/MUA/BSA + 5 μg/mL anti-BSA	10.92	5.83	7.73
Au/MUA/BSA + 20 μg/mL anti-BSA	13.36	7.12	9.69
Au/MUA/BSA + 50 μg/mL anti-BSA	14.27	7.58	10.4
Au/MUA/BSA + 100 μg/mL anti-BSA	15.05	8.02	10.75
Au/MUA/BSA + 200 μg/mL anti-BSA	15.36	7.99	10.92
Au/MUA/BSA + 500 μg/mL anti-BSA	15.22	8.34	11.08

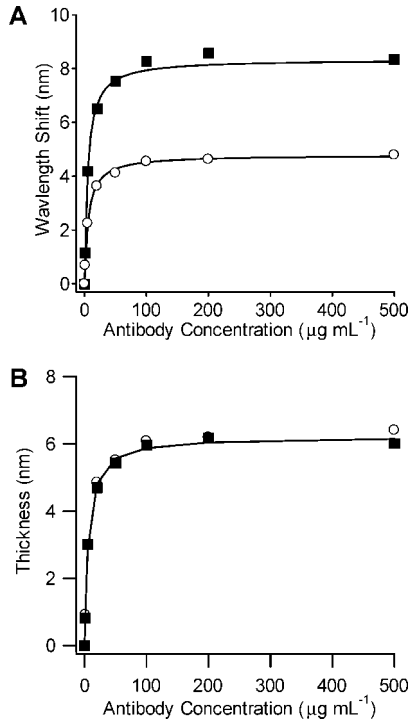

Figure 7. (A) Experimentally measured wavelength shifts in the transmission spectra at $\theta = 15°$ (■) and 50° (○) for antibody−antigen complex versus the concentration of anti-BSA in solution. (B) Equivalent thicknesses for wavelength shift data at $\theta = 15°$ (■) and 50° (○) using calibration constants of 1.38 nm shift/nm thickness and 0.75 nm shift/nm thickness, respectively. The solid line in part B represents the best fit to a Langmuir adsorption isotherm (see text for details).

solution of anti-BSA for 3 h to measure the nonspecific adsorption of anti-BSA at the grating surface. The measured film thickness was 0.86 nm, which was much less than the film thicknesses found when the BSA surface was exposed to anti-BSA solution.

Figure 7A shows the wavelength shifts for the transmission peaks at 15° and 50° angle of incidence measured for the anti-BSA film as a function of the concentration of antibodies in the solution. A similar shape is noted for both curves. The wavelength shift data was then converted to film thickness using the calibration constants determined earlier (see Supporting Information) as 1.38 and 0.75 nm wavelength shift/nm film thickness for the 15° and 50° data, respectively. The results of this calculation are shown in Figure 7B. A near perfect overlap between the two data sets is seen. These shifts were fitted to a one-to-one antigen−antibody binding model and the resulting best-fit curve is shown in the Figure 7B. The one-to-one interaction between the antibodies and BSA molecules can be described by Langmuir type kinetics[56]

$$\text{BSA} + \text{anti-BSA} \underset{k_{-1}}{\overset{k_1}{\leftrightarrow}} \text{BSA} - \text{anti-BSA} \qquad (3)$$

where k_1 and k_{-1} are the forward (association) and reverse (dissociation) rate constants, respectively. If Γ is the surface coverage of the antigen−antibody complex and Γ_{max} is the total surface available to the antibodies, then the relative surface coverage ($\theta = \Gamma/\Gamma_{max}$) at equilibrium is given by the Langmuir adsorption isotherm:

$$\theta = \frac{Kc}{1 + Kc} \qquad (4)$$

where c is the antibody concentration and K (association constant) is the ratio k_1/k_{-1} and is a measure of the affinity of the antibody to the antigen. This simple model has been successfully used to describe the kinetics of immunoreactions as studied by the technique of surface plasmon resonance[57] and other optical techniques.[23,58] The value of K was calculated here as 2.95×10^7 M^{-1}, which is consistent with values of the affinity constant K

(54) Browning-Kelley, M. E.; Wadu-Mesthrige, K.; Hari, V.; Liu, G. Y. *Langmuir* **1997**, *13*, 343–350.
(55) Angeley, D.; Davis, J.; Reitz, G. *Opt. Eng.* **2006**, *45*, 043402.
(56) Kuby, J. *Immunology*, 2nd ed.; W.H. Freeman: New York, 1994.

reported in the literature for the BSA−anti-BSA system as 3.5×10^7, 3.7×10^8, and 0.25×10^8−1.2×10^8 M^{-1}.[59–61]

CONCLUSIONS

We have described a simple, inexpensive, and robust sensor platform based upon surface plasmon resonance enhanced transmission of light at gold-coated grating surfaces. We were able to detect the thickness of ultrathin alkanethiolate self-assembled monolayers as well as the formation of antibody−antigen complexes at gold surfaces using this sensitive detection scheme. Advantages of this detection platform include that it utilizes a simple optical configuration and, as a transmission-based system, possesses enhanced signal-to-noise characteristics when compared to absorbance based SPR sensors. In addition, the ability to tune the wavelength of surface plasmon resonance enhanced transmission by simple grating rotation has numerous potential applications. For example, coupling of surface plasmon modes to semiconductor quantum dots[62] and electronic resonances of molecules[63] as well as surface plasmon enhanced fluorescence[64] requires wavelength tuning.[65] The SPR sensing method described in this work was utilized for ex situ measurements but could easily be extended for in situ sensing and to other systems for biomolecular detection.

(57) Lee, H. J.; Nedelkov, D.; Corn, R. M. *Anal. Chem.* **2006**, *78*, 6504–6510.
(58) Bernard, A.; Bosshard, H. R. *Eur. J. Biochem.* **1995**, *230*, 416–423.

ACKNOWLEDGMENT

The authors gratefully acknowledge Iowa State University for partial support of this work.

SUPPORTING INFORMATION AVAILABLE

Additional information as noted in text. This material is available free of charge via the Internet at http://pubs.acs.org.

Received for review January 8, 2008. Accepted March 7, 2008.

AC800045A

(59) Chiem, N. H.; Harrison, D. J. *Electrophoresis* **1998**, *19*, 3040–3044.
(60) Kierszenbaum, F.; Dandlikre, J.; Dandliker, W. B. *Immunochemistry* **1969**, *6*, 125–137.
(61) Olson, W. C.; Spitznagel, T. M.; Yarmush, M. L. *Mol. Immunol.* **1989**, *26*, 129–136.
(62) Brolo, A. G.; Kwok, S. C.; Cooper, M. D.; Moffitt, M. G.; Wang, C. W.; Gordon, R.; Riordon, J.; Kavanagh, K. L. *J. Phys. Chem. B* **2006**, *110*, 8307–8313.
(63) Zhao, J.; Das, A.; Zhang, X. Y.; Schatz, G. C.; Sligar, S. G.; Van Duyne, R. P. *J. Am. Chem. Soc.* **2006**, *128*, 11004–11005.
(64) Brolo, A. G.; Kwok, S. C.; Moffitt, M. G.; Gordon, R.; Riordon, J.; Kavanagh, K. L. *J. Am. Chem. Soc.* **2005**, *127*, 14936–14941.
(65) Feng, J.; Okamoto, T. *Opt. Lett.* **2005**, *30*, 2302–2304.